Cancer Chemotherapy and Pharmacology (2019) 83:837–848
https://doi.org/10.1007/s00280-019-03793-7

ORIGINAL ARTICLE

Pharmacokinetics, absorption, metabolism, and excretion of [^{14}C] ivosidenib (AG-120) in healthy male subjects

Chandra Prakash[1] · Bin Fan[1] · Syed Altaf[2] · Sam Agresta[3] · Hua Liu[1] · Hua Yang[1]

Received: 18 January 2019 / Accepted: 2 February 2019 / Published online: 13 February 2019

Abstract

Purpose Pharmacokinetics, absorption, metabolism, and excretion of ivosidenib, a mutant isocitrate dehydrogenase-1 inhibitor, were determined in healthy male subjects.

Methods In this open-label phase I study, a single dose of [^{14}C]ivosidenib (500 mg, 200 µCi/subject) was orally administered to eight subjects (CYP2D6 extensive, intermediate, or poor metabolizers) under fasted conditions. Blood, plasma, urine, and fecal samples were assayed for radioactivity and profiled for metabolites. Ivosidenib plasma concentrations were determined using LC–MS/MS. Metabolites were separated using reverse-phase HPLC and analyzed using high-resolution LC–MS and LC–MS/MS.

Results Ivosidenib was readily absorbed and slowly eliminated from plasma. Median T_{max} of both unchanged ivosidenib and radioactivity in plasma was 4 h. Plasma $t_{½}$ values for total radioactivity and ivosidenib were 71.7 and 53.4 h, respectively. The mean $AUC_{0–72}$ blood-to-plasma total radioactivity concentration ratio was 0.565, indicating minimal partitioning to red blood cells. CYP2D6 genotype had no effect on ivosidenib exposure. The mean recovery of radioactivity in excreta was 94.3% over 360 h post-dose; the majority was excreted in feces (77.4 ± 9.62%) with a low percentage recovered in urine (16.9 ± 5.62%), suggesting fecal excretion is the primary route of elimination. Unchanged [^{14}C]ivosidenib accounted for 67.4% of the administered radioactivity in feces. Only [^{14}C]ivosidenib was detected in plasma, representing 92.4% of the total plasma radioactivity. Thirteen metabolites were structurally identified in excreta.

Conclusion Ivosidenib was well-absorbed, slowly metabolized to multiple oxidative metabolites, and eliminated by fecal excretion, with no CYP2D6 effect observed. Unchanged ivosidenib was the only circulating species in plasma.

Keywords Absorption · Metabolism · Excretion · Isocitrate dehydrogenase-1 (IDH1) · Ivosidenib (AG-120) · Metabolites · LC–MS/MS · Cytochrome P450

Introduction

The isocitrate dehydrogenase (IDH) 1, 2, and 3 proteins are metabolic enzymes that catalyze the oxidative decarboxylation of isocitrate to produce CO_2 and alpha-ketoglutarate (α-KG). IDH1 and IDH2 produce the reduced form of nicotinamide adenine dinucleotide phosphate (NADPH), whereas IDH3 produces nicotinamide adenine dinucleotide (NADH).

✉ Chandra Prakash
Chandra.Prakash@agios.com

[1] Agios Pharmaceuticals, Inc., Cambridge, MA 02139, USA

[2] Present Address: Evelo Biosciences, Cambridge, MA, USA

[3] Present Address: Infinity Pharmaceuticals, Inc, Cambridge, MA, USA

IDH1/2 mutations have been identified in a range of solid and hematologic malignancies, including approximately 20% of patients with acute myeloid leukemia (AML) [1]. Cancer-associated mutations in IDH1 and IDH2 are almost always mutually exclusive and occur at very early stages of tumor development suggesting that they promote formation and progression of tumors [2]. Cancer-associated IDH1/2 mutations lead to a gain-of-function, resulting in the abnormal production of (*D*)-2-hydroxyglutarate (2-HG) [3–5]. 2-HG inhibits α-KG dependent dioxygenases, including histone and DNA demethylases that regulate the epigenetic state of cells, impairing cellular differentiation and contributing to oncogenesis [6–9]. Inhibition of the IDH1 mutant protein can suppress 2-HG production and induce cell differentiation [10, 11]. These effects may provide a

therapeutic benefit to patients with IDH1 mutant cancers, including AML.

Ivosidenib (TIBSOVO®), (*S*)-*N*-((*S*)-1-(2-chlorophenyl)-2-((3,3-difluorocyclobutyl)amino)-2-oxoethyl)-1-(4-cyanopyridin-2-yl)-*N*-(5-fluoropyridin-3-yl)-5-oxopyrrolidine-2-carboxamide, is a first-in-class, oral, reversible, potent, targeted inhibitor of the IDH1 mutant protein, for which no significant off-target activity has been observed [10]. Ivosidenib reduced 2-HG levels by > 95% in a tumor xenograft model and induced differentiation ex vivo in mutant IDH1 leukemic cells from patients with AML [10]. Clinical data from two phase I trials in patients with advanced hematologic or solid malignancies harboring an IDH1 mutation have shown that ivosidenib is well-tolerated and has clinical activity in both solid and hematologic tumors [12–14]. Ivosidenib has recently been approved for the treatment of adult patients with relapsed or refractory AML with a susceptible IDH1 mutation as detected by an US Food and Drug Administration (FDA)-approved test [15], and further studies in different patient populations are ongoing.

Ivosidenib is readily absorbed after single and multiple doses both in healthy subjects and in patients with AML across the dose range studied (100 mg twice daily to 1200 mg once daily); time to maximum plasma concentration (T_{max}) was 3–4 h post-dose [16, 17]. In subjects with advanced hematologic malignancies, mean terminal half-life ($t_{½}$) values after single doses were 72–138 h and therefore once-daily dosing was determined to be appropriate [12]. Moderate accumulation was observed after 500 mg once-daily dosing, with mean area under the concentration–time curve (AUC) from time zero to infinity ($AUC_{0-\infty}$) and maximum observed concentration (C_{max}) accumulation ratios of approximately 1.9- and 1.5-fold in advanced hematologic malignancies, respectively [12, 15]. The apparent clearance at steady state (CL_{ss}/F) increased with increasing dose after multiple doses (2.68–6.09 L/h at steady state across the 100 mg twice daily to 1200 mg once daily dose range, unpublished data).

Preliminary in vitro studies using human liver microsomes have suggested that ivosidenib undergoes hepatic metabolism, with the involvement of multiple cytochrome P450 (CYP) enzymes (CYP2B6, CYP2C8, CYP2D6, and CYP3A4, unpublished data). Additional phenotyping experiments using human liver microsomes with chemical inhibitors and recombinant human CYP enzymes suggest that ivosidenib is mainly metabolized by CYP3A4 (unpublished data).

An understanding of the disposition of ivosidenib is important to identify its metabolic profile; to assess the coverage of metabolites in preclinical species used for long-term safety evaluations; to understand the pharmacokinetics (PK) of total radioactivity compared with parent compound and dose recovery; and to understand mechanisms of clearance, which can then inform the potential for drug–drug interactions [18, 19].

The objectives of the present study were to characterize the disposition of ivosidenib in healthy male subjects and to identify and quantify its excretory and circulating metabolites. Safety and tolerability were also evaluated. A single dose of [^{14}C]ivosidenib was orally administered to eight human subjects categorized by CYP2D6 genotype as CYP2D6 extensive metabolizers (EM), intermediate metabolizers (IM), or poor metabolizers (PM). Urine, feces, and plasma were collected and assayed for radioactivity and PK, and profiled for metabolites.

Materials and methods

General chemicals

Commercially obtained chemicals and solvents were of high-performance liquid chromatography (HPLC) or analytical grade. HPLC-grade acetonitrile, methanol, and water, and certified ACS-grade ammonium formate and formic acid were from Fisher Scientific Company (Springfield, NJ, USA).

Radiolabeled study drug

[^{14}C]ivosidenib, labeled at the carboxamide moiety (Fig. 1) was obtained from Moravek Biochemicals, Inc. (Brea, CA, USA). [^{14}C]Ivosidenib hypromellose acetate succinate solid dispersion intermediate was prepared as an oral suspension using methyl cellulose 4000 cP 0.5% w/v and polysorbate 80 0.2% w/v in sterile water as the vehicle. The specific activity of the [^{14}C]ivosidenib hypromellose acetate succinate solid dispersion intermediate was 0.171 mCi/g, and radiopurity was > 99% as confirmed by HPLC with radioactivity detection.

Subjects and dosing

This was a single-center, open-label, non-randomized study conducted in eight healthy male subjects. All subjects provided written informed consent prior to enrollment. The study followed the ethical principles of the Declaration of Helsinki, the International Conference on Harmonization Guideline for Good Clinical Practice, and local regulations (US Code of Federal Regulations Title 21). The protocol, informed consent, and amendments were approved by the Institutional Review Board (Salus IRB; Austin, TX, USA).

After a screening period of up to 27 days (day − 28 to day − 2), eight subjects (categorized by CYP2D6 genotype as 5 EM, 1 IM, and 2 PM) checked into the clinical site on day − 1 for baseline assessments. On the morning of day 1,

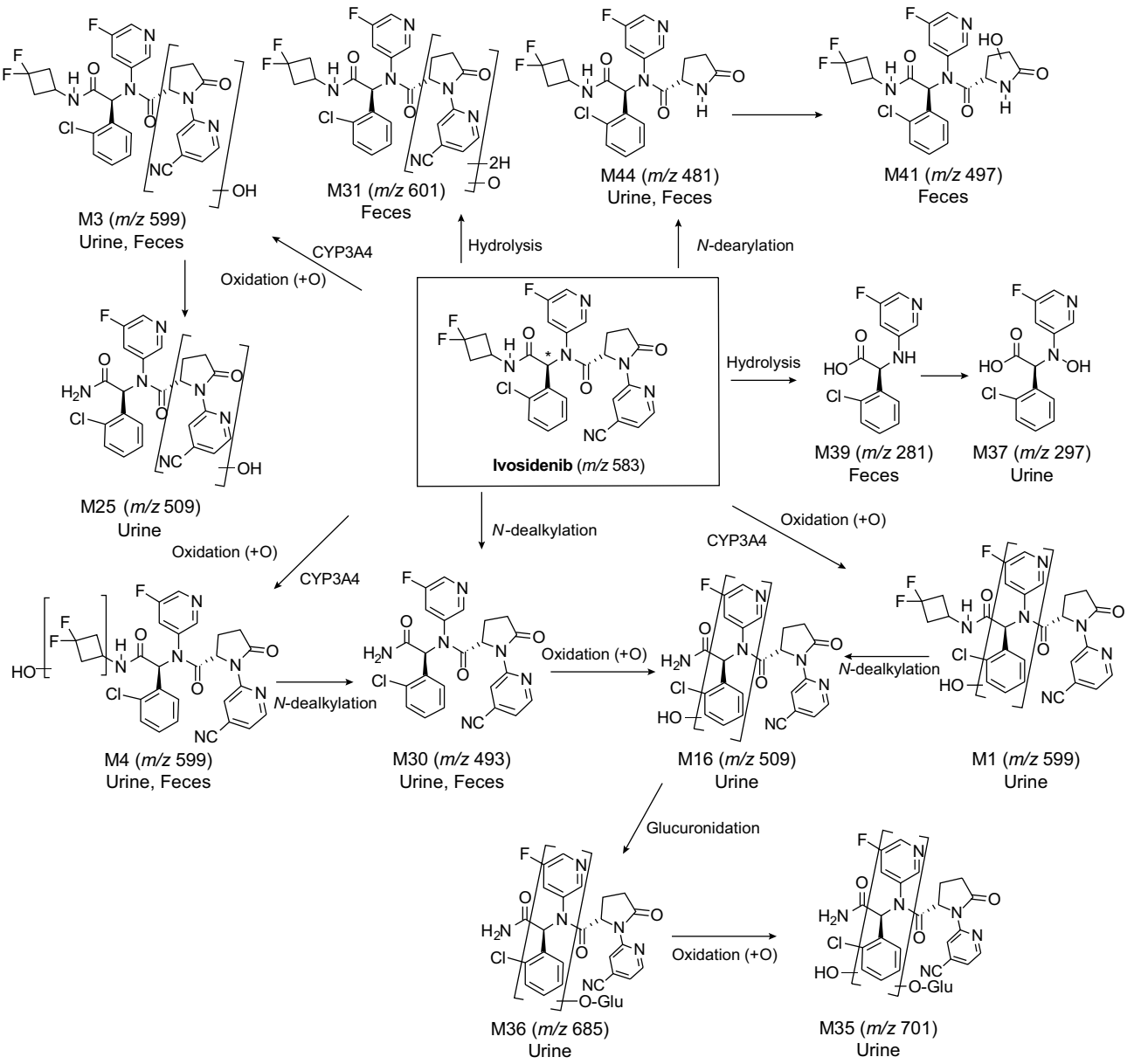

Fig. 1 Proposed metabolic pathways of ivosidenib in humans. Asterisk denotes site of radiolabel. *CYP* cytochrome P450

after an overnight fast, subjects were administered a single oral dose of approximately 500 mg (approximately 200 µCi) [^{14}C]ivosidenib as a suspension in water (50 mL). The dose was immediately followed by two rinses and then by water at room temperature (240 mL total [dose, rinses and water]). Water consumption by subjects was restricted for 1 h prior to dosing and for 2 h post-dosing; at all other times during the study, subjects were allowed to consume water ad libitum.

On the basis of data from a tissue distribution study in male pigmented rats, the overall whole-body radiation dose in a male subject following administration of a single 200 µCi (7.4 MBq) dose of [^{14}C]ivosidenib was calculated to be 30.8 mrem (0.308 mSv), well below the US FDA exposure limit of 3000 mrem after a single dose for human isotope studies (per FDA 21 CFR 361.1) [20].

Sample collection

Serial blood samples were collected on day 1 at pre-dose (hour 0) and 0.5, 1, 2, 3, 4, 6, 8, 12, 24, 48, 72, 96, 120, 144, 168, 240, 336, 408, and 504 h post-dose. Blood was immediately cooled with iced water. Plasma samples were obtained from whole blood by centrifugation at 4 °C within 30 min of collection and kept on ice until aliquoted. Aliquots of blood and plasma were stored at − 20 °C and − 70 °C, respectively. Plasma samples were used to analyze PK and

metabolism, total radioactivity was determined in whole blood and plasma, and additional blood samples were collected for clinical laboratory analyses.

Urine samples were collected on day − 1 (–12 to 0 h) and on day 1 at 0–6, 6–12, 12–24, 24–48, 48–72, and 72–96 h post-dose, and then at 24-h intervals until the subject was discharged. During each time interval, urine samples were pooled, mixed thoroughly, weighed, portioned into aliquots, and stored at ≤ − 70 °C.

Fecal samples were collected on day − 1 (− 24 to 0 h) and on day 1 at 0–24 h post-dose, and then at 24-h intervals until the subject was discharged.

Radioactivity measurements

Dose vial residue analysis

A weighed amount of methanol: water (1:1, v:v; on average 229 g) was added to each empty treatment vial from all subjects to extract any residual radioactivity. Residual radioactivity in each vial was determined by counting duplicate 0.5 g aliquots of each extract by liquid scintillation counting (LSC) using Ultima Gold XR scintillation cocktail (Perkin Elmer; Waltham, MA, USA). Residual radioactivity recovered from each treatment vial was subtracted from the dose administered to the respective subject.

Biological sample (blood, plasma, urine, and feces) analysis

Radioactivity measurements in plasma and urine were performed by LSC. Duplicate samples of plasma (0.4–0.5 g) and urine (0.2–0.5 g) from each sampling time point were added to Ultima Gold XR scintillation cocktail (Perkin Elmer; Waltham, MA, USA) and counted in a liquid scintillation counter. Blood samples were mixed and duplicate weighed aliquots (0.2–0.3 g) were combusted and analyzed by LSC. Fecal samples were combined by subject at 24-h intervals, weighed, and homogenized with methanol:water (1:1, v:v) using a probe-type homogenizer (Polytron Model PT 10-35 [Kinematica; Lucerne, Switzerland]). Triplicate weighed aliquots (0.2–0.3 g) were combusted and analyzed by LSC.

All sample combustions were done in a Model 307 Sample Oxidizer (Packard Instrument Company, Perkin Elmer; Shelton, CT, USA) and the resulting $^{14}CO_2$ was trapped in Carbo-Sorb and diluted with 10 mL PermaFluor®E + scintillation cocktail (Perkin Elmer; Waltham, MA, USA) and counted in a liquid scintillation counter. Oxidation efficiency was evaluated on each day of sample combustion by analyzing a commercial radiolabeled standard both directly in scintillation cocktail and by oxidation. Acceptance criteria were combustion recoveries of 95–105%. All samples were analyzed for radioactivity in a Model 2900TR liquid scintillation counter (Perkin Elmer; Waltham, MA, USA) for at least 5 min or 100,000 counts. Each sample was homogenized or mixed before radioanalysis (unless the entire sample was used for PK/metabolite analysis). All samples were analyzed in duplicate (blood, plasma, and urine) or triplicate (feces).

Scintillation counting data (in disintegration per minute [dpm]) were automatically corrected for counting efficiency using the external standardization technique and an instrument-stored quench curve generated from a series of sealed quenched standards. Radioactivity less than twice the background value was considered to be below the limit of determination. Fecal samples collected prior to dosing were used as the control samples and provided the background count rate.

Mass balance calculations

The actual dose of radioactivity administered to each subject was determined by subtracting the residual radioactivity in the dosing container following dose administration from the total radioactive dose in the dosing container. When determining the amount of radioactivity excreted at each time point as a proportion of the amount administered, the net radioactivity in the actual dose was considered to be 100%. The cumulative excretion of radioactivity in urine and feces during the continuous sampling phase (0–504 h) was calculated by summing the percentages of dose excreted during the 24-h collection intervals.

The amount of radioactivity in plasma at each time point was calculated using the specific activity of the dose administered and was expressed as ng equivalents of parent drug per milliliter.

Preparation of samples for metabolite profiling and identification

Samples were protected from potential degradation by performing procedures under either yellow- or ultraviolet-filtered light.

Plasma

Plasma samples obtained at 2, 4, 8, 12, 24, 48, 72, and 96 h post-dose were pooled by subject to generate a 2–96 h AUC-representative pooled sample using a time-weighted pooling method [21]. The radioactivity in each pooled sample was determined by LSC.

Duplicate 2.5 g portions of each pooled plasma sample were mixed with 6 mL of 1% (v/v) formic acid in acetonitrile, and the samples were sonicated, vortex mixed, and centrifuged. The supernatants were removed and the extraction repeated. The supernatants were combined, and duplicate

aliquots of each sample were analyzed by LSC to determine extraction recoveries. The average extraction recoveries (duplicate samples) ranged from 76.8 to 98.8%. The supernatants from the duplicate samples were combined, evaporated to dryness under nitrogen, and reconstituted in 300 µL of 1:1 (v/v) reverse osmosis water:methanol. Samples were sonicated, vortex mixed, centrifuged, and duplicate aliquots were analyzed by LSC to determine reconstitution recoveries, which ranged from 89.5 to 116%. The reconstituted samples were analyzed by liquid chromatography with tandem mass spectrometry (LC–MS/MS).

Urine

Urine samples collected up to 216 h were pooled by subject to generate a 0–216 h pool. The radioactivity in each pooled sample was determined by LSC. The pooled samples accounted for 90.7–92.4% of the total excreted radioactivity in the urine.

A solid-phase extraction column for each sample was conditioned with 5 mL of methanol, followed by 10 mL of water. Approximately 10 mL of each pooled urine sample was applied and the eluents collected. The columns were then washed with 10 mL of water and the eluents collected, and then eluted with 10 mL of methanol and the eluents collected. Duplicate aliquots of each eluent were analyzed by LSC to determine recoveries. The methanol eluent recoveries ranged from 99.7 to 105%. The methanol eluents were evaporated to dryness and reconstituted in 300 µL of reverse osmosis water and 150 µL of methanol. The reconstituted samples were sonicated, vortex mixed, and centrifuged, and duplicate aliquots were analyzed by LSC to determine reconstitution recoveries, which ranged from 89.2 to 130%. The reconstituted samples were analyzed by LC–MS/MS.

Feces

Feces samples were pooled by subject to generate 0–168 h (subjects 101 and 105), 0–264 h (subject 102), 0–192 h (subject 103), 0–96 h (subject 104), 0–240 h (subject 106), 0–144 h (subject 107), and 0–120 h (subject 108) pooled samples. Aliquots of each sample were combusted and analyzed by LSC to determine the radioactivity. The pooled samples accounted for 93.2–96.3% of the total radioactivity excreted in the feces.

Approximately 2.5 g of each pooled feces sample was combined with 6 mL of 1% (v/v) formic acid in acetonitrile, sonicated, vortex mixed, and centrifuged. The supernatants were removed and the extraction repeated. The supernatants were combined, and duplicate aliquots of each sample were analyzed by LSC to determine extraction recoveries, which ranged from 72.7 to 97.7%. The supernatants were evaporated to dryness under nitrogen and reconstituted in 500 µL of 2:2:1 (v/v/v) reverse osmosis water: 1% (v/v) formic acid in acetonitrile:methanol. Samples were sonicated, vortex mixed, centrifuged, and duplicate aliquots were analyzed by LSC to determine reconstitution recoveries, which ranged from 98.7 to 106%. The reconstituted samples were analyzed by liquid chromatography with mass spectrometry (LC–MS) and LC–MS/MS.

HPLC

The HPLC system consisted of an Agilent 1200 binary delivery pump, membrane degasser, HiP-ALS SL + autosampler and FC/ALS thermostat (6 °C or 15 °C) (Agilent; Lexington, MA, USA) and a LEAP Technologies (Ringwood, Australia) PAL HTS-xt fraction collector. Chromatography was performed on a Waters Atlantis T3, (4.6 × 250 mm, 5 µm; Waters Corporation, Peabody, MA, USA) and a Phenomenex C18 guard column (4 × 3 mm; Torrance, CA, USA) with a mobile phase containing a mixture of 0.1% (v/v) formic acid in water (solvent *A*) and acetonitrile (solvent *B*). The mobile phase was initially composed of *A*/*B* (90:10), was then linearly programmed to *A*/*B* (30:70) over 48.9 min, and then changed to *A*/*B* (5:95) over 0.1 min, followed by an *A*/*B* (5:95) 5 min wash. Then, the mobile phase composition was returned to the starting solvent mixture over 0.1 min. The system was allowed to equilibrate for approximately 5 min before making the next injection. The flow rate was 1.0 mL/min and separation was at ambient temperature.

LC–MS/MS

Identification of the metabolites was performed on an Agilent 6530 Q-TOF with dual electrospray ionization source (Agilent, Lexington, MA, USA). The effluent from the HPLC column was split in a 1:3 ratio to mass spectrometer and fraction collector. The fractions were collected at 10 s intervals into 96-well plates containing solid scintillant. Radioactivity in each well was determined using TopCount analysis, and radiochromatograms were generated on the basis of radioactivity counts. The MS interface was set at 4000 V and the spectrometer was operated with capillary temperature set at 325 °C. Mass spectrometric data analysis was performed using Xcalibur v.1.4 vSR1 (Thermo Electron, Waltham, MA, USA).

Quantitative assessment of metabolite profiles

Peaks in the ^{14}C-chromatograms were integrated using QuantaSmart software (Perkin Elmer; Waltham, MA, USA). Quantities of individual radiolabeled components were calculated from the relative peak areas and the concentrations (plasma) or amounts (urine, feces) of total ^{14}C-labeled components in the respective original sample pools. Peaks were

quantitated as follows: a background of 3 cpm was applied to all chromatograms. The net amount of radioactivity in each peak was expressed as a percentage of total radioactivity in the chromatogram or sample. Metabolite profiles in plasma are reported as a percentage of total radioactivity. The relative abundance of metabolites in urine and feces was based on the cumulative percentage of recovered dose in that matrix and was calculated using the following equation:

Extrapolated % of total radioactive dose
= (% of total radioactivity in peak/100)
× total percent of recovered dose in excreta.

LC–MS/MS determination of ivosidenib in plasma and urine

Plasma and urine concentrations of ivosidenib were determined by Covance Labs (West Trenton, NJ, USA) using validated LC–MS/MS methods. The assay had a dynamic range of 50 ng/mL (lower limit of quantitation [LLOQ])–50,000 ng/mL for plasma and 1 ng/mL (LLOQ)–1000 ng/mL for urine using an aliquot volume of 100 µL each.

Pharmacokinetic analysis

PK parameters were determined using Phoenix WinNonlin version 6.2.1 (Pharsight Corporation [now Certara; Princeton, NJ, USA]). C_{max} of ivosidenib in plasma and total radioactivity (parent drug equivalents) in plasma and blood were estimated directly from the experimental data, with T_{max} defined as the time of first occurrence of C_{max}. Terminal phase rate constants (k_{el}) were estimated using least squares regression analysis of the plasma concentration–time data obtained during the terminal log-linear phase. Half-life ($t_{½}$) was calculated as $0.693/k_{el}$. AUC from time 0 to the last time with a measurable concentration (AUC_{0-t}) was estimated using the linear trapezoidal rule. AUC from time t to infinity ($AUC_{t-\infty}$) was estimated as C_{est}/k_{el} where C_{est} represents the estimated concentration at time t on the basis of the aforementioned regression analysis. Mean blood-to-plasma total radioactivity concentration ratios were calculated to determine the association of radioactivity with red blood cells (RBCs). The effect of CYP2D6 genotype on the PK of total radioactivity and unchanged ivosidenib in healthy male subjects was assessed by comparing the PK between subjects with CYP2D6 PM genotypes and non-PM genotypes.

Safety assessments

Safety assessments (including vital signs, laboratory evaluations, electrocardiograms, and adverse events) were conducted throughout the study. The nature, time of onset, duration, and severity were documented, together with an investigator's opinion of the relationship to ivosidenib. Any clinically significant abnormalities found during the course of the study were followed up until they returned to normal or could be clinically explained.

Results

Demographics, disposition, and safety

The subjects enrolled were healthy males aged between 25 and 53 years, inclusive, with a mean [standard deviation (SD)] body mass index of 23.98 (4.481) kg/m^2, mean (SD) body weight of 75.7 (10.01) kg, vital signs within the normal range, and no clinically significant abnormalities. Four subjects were white and four subjects were black or African American. There were no clinically significant safety findings during the study and no subjects discontinued because of an adverse event. Two subjects experienced four mild to moderate (grade 1) adverse events that were suspected to be related to ivosidenib (abnormal dreams, muscle spasms, increased erection, and diarrhea). There were no clinically significant changes in vital signs, electrocardiography, clinical laboratory evaluations, and physical examinations.

Dose administration

The doses administered ranged from 476 to 500 mg (166–174 µCi), and were close to the target dose of 500 mg (200 µCi). Doses were calculated using the specific activity of [^{14}C]ivosidenib in the dose formulation (0.171 mCi/g), the individual drug concentration, and radioactivity concentrations.

Mass balance of radioactivity

The percentages of radioactive dose recovered in urine and feces are presented in Table 1, and the cumulative percentage recovery in Fig. 2. Most of the administered radioactivity was recovered in the first 192 h post-dose (88.2 ± 8.38%). The overall mean (± SD) recovery of radioactivity in urine and feces samples was 94.3 ± 6.8% over 360 h post-dose, with recovery in individual subjects ranging from 82.1 to 106%. There was no difference in the excretion pattern of radioactivity between CYP2D6 PM and non-PM (Table 1).

Table 1 Recovery (%) of radioactive dose over 0–360 h

Subject	*CYP2D6* genotype	Recovery of radioactive dose, %		
		Urine	Feces	Total
101	EM	24.0	58.2	82.1
102	EM	25.6	69.9	95.4
103	EM	15.3	76.6	91.9
104	IM	10.0	85.8	95.8
105	EM	18.8	87.0	105.8
106	EM	14.6	76.2	90.8
107	PM	16.4	82.5	98.9
108	PM	10.8	82.9	93.7
Mean ± SD	–	16.9 ± 5.62	77.4 ± 9.62	94.3 ± 6.8

CYP cytochrome P450, *EM* extensive metabolizer, *IM* intermediate metabolizer, *PM* poor metabolizer, *SD* standard deviation

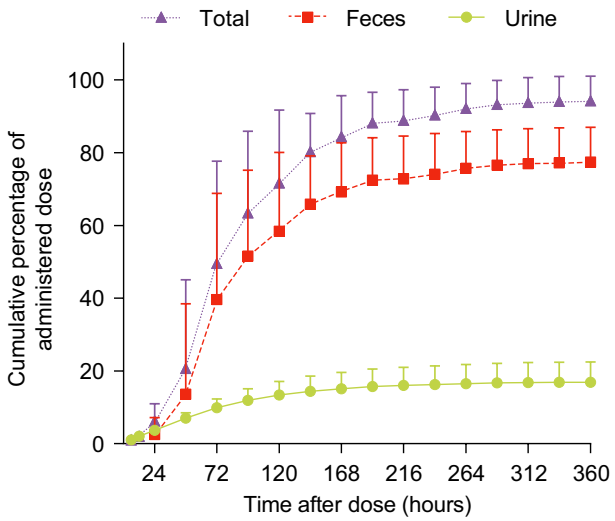

Fig. 2 Mean (+standard deviation) cumulative urinary, fecal, and total excretion of radioactivity after a single oral dose of 500 mg [^{14}C]ivosidenib

Pharmacokinetics of radioactivity and ivosidenib

There was no difference in the PK of radioactivity between CYP2D6 PM and non-PM; therefore, mean PK data for total radioactivity in blood and plasma and for ivosidenib in plasma for all eight subjects are summarized in Table 2, and concentration–time profiles are shown in Fig. 3. Radioactivity was detected in plasma and whole blood at a median T_{max} of 4 and 5 h, respectively. C_{max} of ivosidenib in plasma was reached at 4 h. After reaching C_{max}, ivosidenib and total radioactivity steadily declined, generally in a multiphasic manner, with arithmetic mean (± SD) $t_{½}$ values of 53.4 ± 12.0 and 71.7 ± 16.6 h, respectively.

The mean C_{max}, $AUC_{0–72}$, and $AUC_{0–\infty}$ values for unchanged ivosidenib were only slightly lower than those for total radioactivity in plasma, suggesting that most of the circulating radioactivity was comprised of unchanged ivosidenib. The geometric mean $AUC_{0–72}$ blood-to-plasma ratio was 0.565, indicating minimal association of radioactivity with RBCs. Levels of radioactivity were below the LLOQ for all subjects by 336 h (14 days) post-dose in blood and 504 h (21 days) post-dose in plasma. Moderate to high between-subject variability was observed in C_{max} and AUC values, demonstrated by CV% values ranging from 23.6 to 65.6%.

The arithmetic mean renal clearance (CL_R) of ivosidenib was 0.537 L/h, less than the typical glomerular filtration rate of approximately 7.5 L/h.

Metabolite profiles

The limit of quantitation for radioactivity in all matrices was set at 1% of the total radioactivity injected and 10 cpm peak height; radioactive peaks less than these are reported as not detected. The relative abundance of metabolites as percentages of radioactive dose in urine, feces, and plasma are presented in Table 3.

Urine

A total of 14 radioactive peaks were detected in the radiochromatogram of human urine (Fig. 4a). Unchanged [^{14}C]ivosidenib and ten metabolites (M1, M3, M4, M16, M25, M30, M35, M36, M37, and M44) were tentatively identified by LC–MS/MS. Unchanged [^{14}C]ivosidenib was the most abundant radioactive component in pooled urine, representing 9.92% of the total recovered dose. M1 was the next most abundant component, representing 3.11% of the total recovered dose. The other 12 metabolites (M3, M4, M16, M25, M30, M35, M36, M37, M38, M40, M42, and M44) each represented ≤ 1% of the total dose. [^{14}C]Ivosidenib and the identified metabolites accounted for a mean of 92.9% of the radioactivity (15.9% of the dose) recovered in the urine.

Feces

A total of nine radioactive peaks were detected in the radiochromatogram of human feces (Fig. 4b). Unchanged [^{14}C]ivosidenib and seven metabolites (M3, M4, M30, M31, M39, M41, and M44) were tentatively identified. Unchanged [^{14}C]ivosidenib was the most abundant radioactive component in pooled human feces, representing approximately 67.4% of the total recovered dose. M3, M44, and M31 were the most abundant metabolites in human feces, representing 2.58, 1.74, and 1.28% of the total dose, respectively. The other five metabolites (M4, M30, M39, M41, and M43),

Table 2 Pharmacokinetic parameters for total radioactivity in blood and plasma, and for ivosidenib in plasma and urine ($N=8$)

Parameter	Ivosidenib		Total radioactivity	
	Urine	Plasma	Plasma	Whole blood
AUC_{0-72}, h·ng/mL	–	43,500 (45.4)	53,800 (42.0)	30,400 (37.7)
AUC_{0-t}, h·ng/mL	–	72,400 (56.9)	99,900 (56.2)	44,800 (65.6)
$AUC_{0-\infty}$, h·ng/mL	–	79,300 (54.0)	10,8000 (51.9)	79,200 (42.9)[a]
C_{max}, ng/mL	–	990 (28.5)	1160 (23.8)	635 (23.6)
T_{max}, h	–	4.00 (3.05–48.00)	4.00 (3.00–48.00)	5.00 (3.00–72.00)
λ_z, h^{-1}	–	0.0133 (23.2)	0.00989 (23.8)	0.0114 (38.7)
$t_{½}$, h	–	53.4 (12.0)	71.7 (16.6)	64.9 (26.1)
CL/*F*, L/h	–	6.31 (54.0)	NA	NA
V_z/F, L	–	475 (43.0)	NA	NA
Blood/plasma total radioactivity AUC_{0-72} ratio	–	–	–	0.565 (5.4)
Blood/plasma total radioactivity $AUC_{0-\infty}$ ratio	–	–	–	0.556 (7.2)[a]
Ae, mg	42.2 (14.1)	–	–	–
% excreted	8.44 (2.83)	–	–	–
CL_R, L/h	0.537 (0.189)	–	–	–

C_{max} and AUC values are expressed as ng equiv/mL and ng equiv h/mL, respectively

Ae amount of drug excreted in urine, AUC_{0-t} area under the concentration–time curve from time zero to the time of the last measurable concentration, $AUC_{0-\infty}$ area under the concentration–time curve from time zero to infinity with extrapolation of the terminal phase, *CL/F* apparent total plasma clearance, CL_R renal clearance, C_{max} maximum observed concentration, *CV* coefficient of variation, *F* absolute bioavailability, *NA* not applicable, T_{max} time to reach C_{max}, $t_{½}$ elimination half-life associated with the terminal slope, V_z/F apparent terminal volume of distribution, *% excreted* percentage excreted in urine, λ_z apparent terminal elimination rate constant. T_{max} is presented as median (range) and $t_{½}$, Ae, % excreted, and CL_R as arithmetic mean (standard deviation). All other values are presented as geometric mean (CV%)

[a]$N=5$

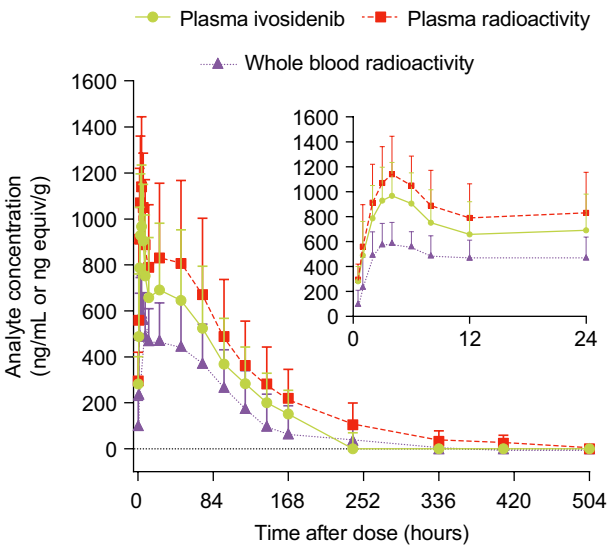

Fig. 3 Mean (+standard deviation) concentration–time profiles of total radioactivity in blood and plasma, and ivosidenib in plasma, after a single oral dose of 500 mg [^{14}C]ivosidenib

each represented ≤0.5% of the total dose. Ivosidenib and the identified metabolites accounted for a mean of 95.6% of the excreted radioactivity (74.0% of the dose) recovered in the feces.

Plasma

[^{14}C]Ivosidenib was the only radioactive component detected in AUC_{2-96} pooled plasma samples, with no radioactive metabolites detected in samples from any of the eight subjects (Fig. 4c). On average, [^{14}C]ivosidenib represented 92.4% of the radioactivity in these samples.

Identification of metabolites

The structures of metabolites were elucidated by electrospray LC–MS/MS using a combination of Q1 and CID product ion (MS^2) scanning techniques [22]. The CID product ion spectrum of ivosidenib protonated molecular ion [MH^+] at *m/z* 583 gave the characteristic fragment ions at *m/z* 476, 370, 214, and 186. The fragment ion at *m/z* 476 resulted from loss of the difluoro-cyclobutylamine moiety after

Table 3 Mean relative abundance (% dose) of ivosidenib and metabolites in urine and feces

Metabolite designation	Retention time, min	Extrapolated percentage of dose		
		Urine	Feces	Total
M35	19.67	0.12	–	0.12
M36	20.67–20.83	0.55	–	0.55
M37	21.67	0.05	–	0.05
M38	24.67	0.03	–	0.03
M39	25.67	–	0.16	0.16
M16	26.33	0.03	–	0.03
M40	27.83	0.15	–	0.15
M41	28.17	–	0.51	0.51
M42	28.67	0.04	–	0.04
M43	29.67	–	0.10	0.10
M25	30.67	0.03	–	0.03
M44	31.00–31.17	0.08	1.74	1.82
M30	34.00–34.33	0.58	0.18	0.76
M31	35.00	–	1.28	1.28
M1	35.83–36.00	3.11	–	3.11
M3	39.33–39.83	0.18	2.58	2.76
M4	39.67–40.17	1.04	0.22	1.26
Ivosidenib	43.67–44.17	9.92	67.4	77.3

cleavage of the amide bond. Cleavage of the other amide bond produced the fragment ion at *m/z* 370 representing the chorophenyl-(difluorocyclobutyl)amino-2-oxoethyl-*N*-(5-fluoropyridin-3-yl) moiety. The fragment ion at *m/z* 214 represented the pyridinyl-pyrrolidone moiety and the ion at *m/z* 186 was formed by loss of CO from the fragment ion at *m/z* 214. Analogous fragment ions were observed in the mass spectra of the metabolites, which allowed the localization of metabolic changes to the cyclobutyl, pyridinyl-pyrrolidone, or cyanopyridine parts of the molecule. This information, together with accurate mass data on [MH^+] ions and fragments, allowed the assignment of the metabolite structures as shown in Fig. 1.

Proposed biotransformation pathways

The proposed biotransformation pathways for [^{14}C]ivosidenib are shown in Fig. 1. The primary metabolic pathways for [^{14}C]ivosidenib in human male subjects were due to oxidation, N-dealkylation, N-dearylation, and amide hydrolysis. The other metabolites were a result of the combination of these primary pathways and glucuronide conjugation. The contributions of different biotransformation pathways to the metabolism of ivosidenib were estimated on the basis of the percentage of dose accounted for by the respective metabolites in urine and feces. Oxidation at the chlorobenzyl-*N*-5-fluoropyridinyl moiety accounted for approximately 3.81% of the dose and resulted in the formation of four identified metabolites (M1, M16, M35, and M36). Oxidation at the cyanopyridinyl-pyrrolidone moiety accounted for approximately 2.79% of the dose and resulted in the formation of two metabolites (M3 and M25). Oxidation at the difluoro-cyclobutyl moiety accounted for approximately 2.03% of the dose and resulted in the formation of two metabolites (M4 and M30). Amide hydrolysis, which accounted for 1.49% of the dose, resulted in the formation of M31, M37, and M39. *N*-dearylation of the cyanopyridine moiety accounted for 2.33% of the dose and resulted in the formation of M41 and M44 (Fig. 1). Unchanged [^{14}C]ivosidenib accounted for approximately 9.92 and 67.4% of the total recovered dose in urine and feces, respectively.

Discussion

In this study, we characterized the routes of elimination, metabolism, excretion, and mass balance of [^{14}C]ivosidenib after a single oral dose of approximately 500 mg to humans. A radioactivity dose of 200 µCi [^{14}C]ivosidenib was selected for this study on the basis of radioactivity dosimetry estimations from the tissue distribution of [^{14}C]ivosidenib in rats. The administered radioactive dose was almost completely (~ 94%) recovered in humans, indicating that the mass balance of ivosidenib was well-characterized. A major portion of the administered radioactive dose was eliminated via the fecal route (approximately 77%), and urinary elimination accounted for approximately 17% of the dose.

Ivosidenib was readily absorbed following the administration of a single dose of [^{14}C]ivosidenib, and was slowly eliminated from plasma. The median T_{max} values of unchanged ivosidenib and radioactivity in plasma were similar (4 h). After reaching C_{max}, ivosidenib and total radioactivity in plasma declined in a multiphasic manner, which indicated an approximately parallel decrease in unchanged ivosidenib and total radioactivity, and no significant accumulation of metabolites in the body. Absorbed ivosidenib was distributed into the tissues and was metabolized slowly. The apparent terminal volume of distribution was high, and the apparent clearance was low. The geometric mean plasma ivosidenib/plasma total radioactivity ratio for $AUC_{0–72}$ was 0.810, suggesting that the majority of circulating radioactivity was comprised of unchanged ivosidenib. The geometric mean $AUC_{0–72}$ blood/plasma ratio of 0.565 suggests minimal association of radioactivity with RBCs. No marked difference in systemic exposure to ivosidenib, as assessed by mean AUC and C_{max} values, was observed between CYP2D6 PM and non-PM genotypes, and any differences observed were within the general variability among the individual subjects. These data suggest that CYP2D6 plays a minor role, if any, in the elimination of ivosidenib.

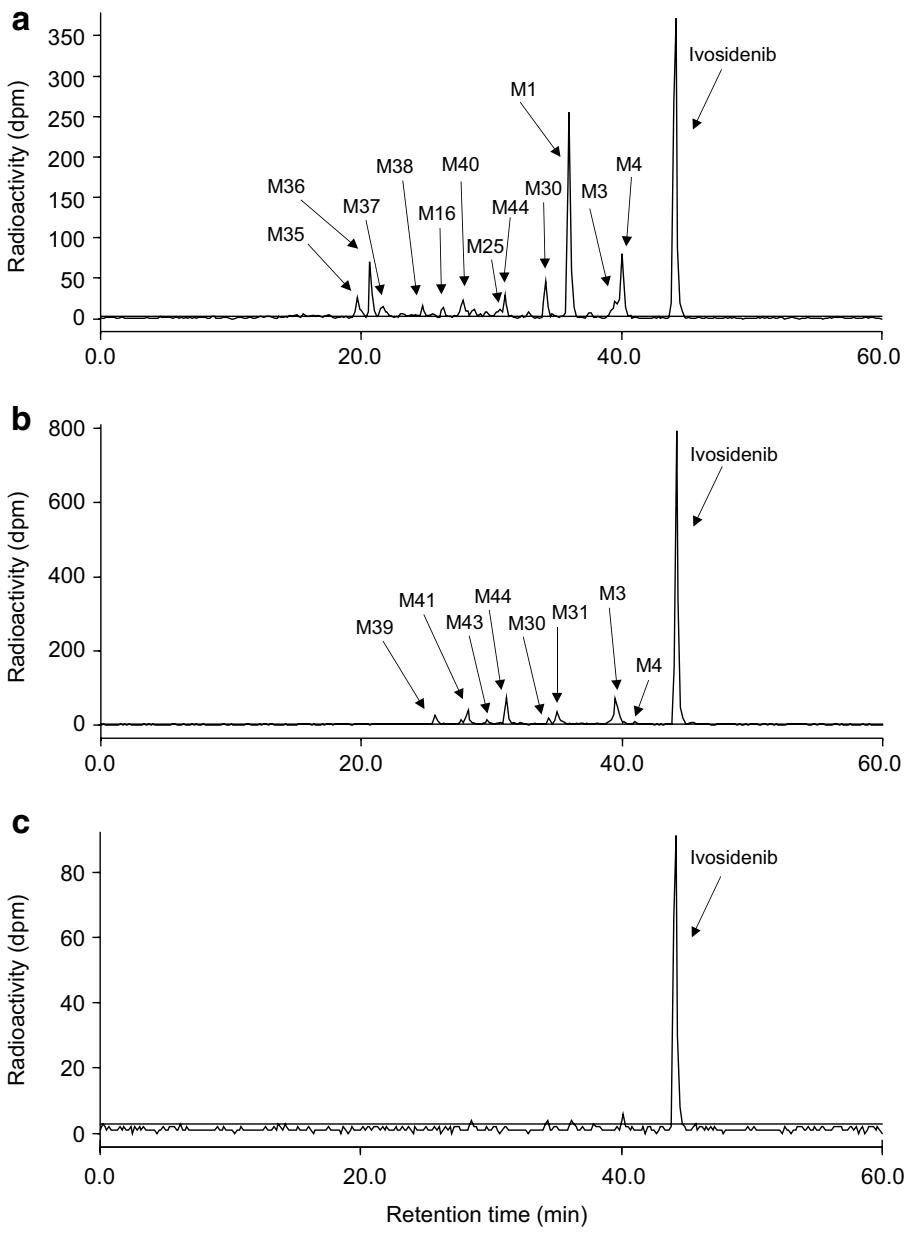

Fig. 4 Representative metabolite profiles in urine, feces, and plasma after a single oral dose of 500 mg [^{14}C]ivosidenib. **a** Urine pool from the 0–216 h interval. **b** Feces pool across the 0–264 h interval. **c** Plasma AUC pool. The unit of radioactivity as shown on the *y*-axis is disintegrations per minute (dpm) per mL of column effluent

Unchanged [^{14}C]ivosidenib accounted for, on average, 67.4% of the total recovered dose in feces. These data suggest that at least 32.6% of the dose was absorbed from the suspension (assuming that non-absorption was responsible for all of the 67.4% of the total recovered dose excreted in feces as unchanged drug). These results are consistent with data from the preclinical toxicology studies in rats, in which ivosidenib was also eliminated primarily in feces (unpublished data). The half-life of ivosidenib observed in this study was similar to that in the phase I study in healthy subjects [17]. However, compared with the current study in which healthy subjects received a suspension of powder made by dry blending, the plasma levels of ivosidenib were 1.8-fold higher in clinical trials conducted in healthy subjects who were administered tablets [17]. These data suggest that > 58% of the dose was absorbed in healthy subjects when tablets were administered under fasting conditions. Lower absorption of dry blended formulations compared with commercial tablet/capsule formulations has been observed for other drugs, such as sonidegib [23].

The urine and feces radiochromatograms indicated that ivosidenib is slowly metabolized after a single oral dose in human male subjects. Ivosidenib and a total of 13 metabolites were structurally identified using LC–MS and LC–MS/MS. Unchanged [^{14}C]ivosidenib accounted for, on average, 77.3% of the total recovered radioactivity. Only [^{14}C]

ivosidenib was detected in plasma, representing on average 92.4% of the total radioactivity in pooled plasma samples from the human male subjects.

The elimination of absorbed ivosidenib occurred predominantly by metabolism; the mean CL_R of ivosidenib was less than the typical glomerular filtration rate. The current study indicates that the primary metabolic clearance of ivosidenib is achieved through oxidative (68%), dearylation (18%), and amide hydrolysis (12%) pathways.

In vitro studies using human liver microsomes with chemical inhibitors and recombinant human CYP enzymes have suggested that the oxygenated metabolites M1, M3, and M4 are formed by CYP3A4, and that CYP3A5 does not play any role in their formation (unpublished data). Because the dealkylated metabolite M30 and the dearylated metabolite M44 were not detected in vitro, it was speculated that these metabolites are formed by further metabolism of oxygenated metabolites M4 and M3, respectively. These results are in agreement with those of phase I clinical trials evaluating CYP3A4 involvement in ivosidenib metabolism via co-administration of the potent CYP3A4 inhibitor itraconazole [17], in which the ivosidenib AUC was increased by 169% with itraconazole co-administration. This AUC change is consistent with CYP3A4 involvement of approximately 65% in clearance.

In conclusion, this open-label phase I study has provided a good understanding of ivosidenib PK, metabolism, and clearance mechanisms in humans. Ivosidenib is well-absorbed and slowly metabolized to multiple oxidative metabolites, primarily by CYP3A4, and eliminated primarily via the fecal route. Unchanged parent ivosidenib is the only circulating species in plasma.

Acknowledgements The authors would like to acknowledge the contributions of Covance Clinical for conducting the study and Covance Drug Metabolism and Pharmacokinetics Department for ADME profiling. We would like to also thank Gary Conner, Camelia Gliser, Shijie Zhang, and Huayu Xiong (Agios) for their help in conducting the study; and Christine Ingleby Ph.D. (of Excel Medical Affairs, Horsham, UK, funded by Agios) and Allyson Bower (Agios) for editorial assistance with the manuscript. We would also like to thank the volunteers who participated in the study.

Author contributions All authors performed data analysis and interpretation, as well as manuscript writing, review, and approval.

Funding This study was supported financially by Agios Pharmaceuticals, Inc., Cambridge, MA, USA.

Compliance with ethical standards

Conflict of interest All authors were paid employees of Agios Pharmaceuticals, Inc., Cambridge, MA, USA at the time of the study.

Ethical approval All procedures performed in studies involving human participants were in accordance with the ethical standards of the institutional and/or national research committee and with the 1964 Helsinki Declaration and its later amendments or comparable ethical standards.

Informed consent Informed consent was obtained from all individual participants included in the study.

References

1. Medeiros BC, Fathi AT, DiNardo CD, Pollyea DA, Chan SM, Swords R (2017) Isocitrate dehydrogenase mutations in myeloid malignancies. Leukemia 31:272–281. https://doi.org/10.1038/leu.2016.275
2. Dang L, Su SM (2017) Isocitrate dehydrogenase mutation and (R)-2-hydroxyglutarate: from basic discovery to therapeutics development. Annu Rev Biochem 86:305–331. https://doi.org/10.1146/annurev-biochem-061516-044732
3. Dang L, White DW, Gross S, Bennett BD, Bittinger MA, Driggers EM, Fantin VR, Jang HG, Jin S, Keenan MC, Marks KM, Prins RM, Ward PS, Yen KE, Liau LM, Rabinowitz JD, Cantley LC, Thompson CB, Vander Heiden MG, Su SM (2009) Cancer-associated IDH1 mutations produce 2-hydroxyglutarate. Nature 462:739–744. https://doi.org/10.1038/nature08617
4. Ward PS, Patel J, Wise DR, Abdel-Wahab O, Bennett BD, Coller HA, Cross JR, Fantin VR, Hedvat CV, Perl AE, Rabinowitz JD, Carroll M, Su SM, Sharp KA, Levine RL, Thompson CB (2010) The common feature of leukemia-associated IDH1 and IDH2 mutations is a neomorphic enzyme activity converting α-ketoglutarate to 2-hydroxyglutarate. Cancer Cell 17:225–234. https://doi.org/10.1016/j.ccr.2010.01.020
5. Gross S, Cairns RA, Minden MD, Driggers EM, Bittinger MA, Jang HG, Sasaki M, Jin S, Schenkein DP, Su SM, Dang L, Fantin VR, Mak TW (2010) Cancer-associated metabolite 2-hydroxyglutarate accumulates in acute myelogenous leukemia with isocitrate dehydrogenase 1 and 2 mutations. J Exp Med 207:339–344. https://doi.org/10.1084/jem.20092506
6. Chowdhury R, Yeoh KK, Tian YM, Hillringhaus L, Bagg EA, Rose NR, Leung IK, Li XS, Woon EC, Yang M, McDonough MA, King ON, Clifton IJ, Klose RJ, Claridge TD, Ratcliffe PJ, Schofield CJ, Kawamura A (2011) The oncometabolite 2-hydroxyglutarate inhibits histone lysine demethylases. EMBO Rep 12:463–469. https://doi.org/10.1038/embor.2011.43
7. Lu C, Ward PS, Kapoor GS, Rohle D, Turcan S, Abdel-Wahab O, Edwards CR, Khanin R, Figueroa ME, Melnick A, Wellen KE, O'Rourke DM, Berger SL, Chan TA, Levine RL, Mellinghoff IK, Thompson CB (2012) IDH mutation impairs histone demethylation and results in a block to cell differentiation. Nature 483:474–478. https://doi.org/10.1038/nature10860
8. Xu W, Yang H, Liu Y, Yang Y, Wang P, Kim SH, Ito S, Yang C, Xiao MT, Liu LX, Jiang WQ, Liu J, Zhang JY, Wang B, Frye S, Zhang Y, Xu YH, Lei QY, Guan KL, Zhao SM, Xiong Y (2011) Oncometabolite 2-hydroxyglutarate is a competitive inhibitor of alpha-ketoglutarate-dependent dioxygenases. Cancer Cell 19:17–30. https://doi.org/10.1016/j.ccr.2010.12.014
9. Figueroa ME, Abdel-Wahab O, Lu C, Ward PS, Patel J, Shih A, Li Y, Bhagwat N, Vasanthakumar A, Fernandez HF, Tallman MS, Sun Z, Wolniak K, Peeters JK, Liu W, Choe SE, Fantin VR, Paietta E, Lowenberg B, Licht JD, Godley LA, Delwel R, Valk PJ, Thompson CB, Levine RL, Melnick A (2010) Leukemic IDH1 and IDH2 mutations result in a hypermethylation phenotype, disrupt TET2 function, and impair hematopoietic differentiation. Cancer Cell 18:553–567. https://doi.org/10.1016/j.ccr.2010.11.015
10. Popovici-Muller J, Lemieux RM, Artin E, Saunders JO, Salituro FG, Travins J, Cianchetta G, Cai Z, Zhou D, Cui D, Chen

P, Straley K, Tobin E, Wang F, David MD, Penard-Lacronique V, Quivoron C, Saada V, de Botton S, Gross S, Dang L, Yang H, Utley L, Chen Y, Kim H, Jin S, Gu Z, Yao G, Luo Z, Lv X, Fang C, Yan L, Olaharski A, Silverman L, Biller S, Su SM, Yen K (2018) Discovery of AG-120 (ivosidenib): a first-in-class mutant IDH1 inhibitor for the treatment of IDH1 mutant cancers. ACS Med Chem Lett 9:300–305. https://doi.org/10.1021/acsmedchemlett.7b00421

11. Rohle D, Popovici-Muller J, Palaskas N, Turcan S, Grommes C, Campos C, Tsoi J, Clark O, Oldrini B, Komisopoulou E, Kunii K, Pedraza A, Schalm S, Silverman L, Miller A, Wang F, Yang H, Chen Y, Kernytsky A, Rosenblum MK, Liu W, Biller SA, Su SM, Brennan CW, Chan TA, Graeber TG, Yen KE, Mellinghoff IK (2013) An inhibitor of mutant IDH1 delays growth and promotes differentiation of glioma cells. Science 340:626–630. https://doi.org/10.1126/science.1236062
12. DiNardo CD, Stein EM, de Botton S, Roboz GJ, Altman JK, Mims AS, Swords R, Collins RH, Mannis GN, Pollyea DA, Donnellan W, Fathi AT, Pigneux A, Erba HP, Prince GT, Stein AS, Uy GL, Foran JM, Traer E, Stuart RK, Arellano ML, Slack JL, Sekeres MA, Willekens C, Choe S, Wang H, Zhang V, Yen KE, Kapsalis SM, Yang H, Dai D, Fan B, Goldwasser M, Liu H, Agresta S, Wu B, Attar EC, Tallman MS, Stone RM, Kantarjian HM (2018) Durable remissions with ivosidenib in IDH1-mutated relapsed or refractory AML. N Engl J Med 378:2386–2398. https://doi.org/10.1056/NEJMoa1716984
13. Mellinghoff IK, Touat M, Maher E, de la Fuente M, Cloughesy TF, Holdhoff M, Cote GM, Burris H, Janku F, Huang R, Young RJ, Ellingson B, Nimkar T, Jiang L, Ishii Y, Choe S, Fan B, Steelman L, Yen K, Bowden C, Pandya S, Wen PY (2017) AG-120, a first-in-class mutant IDH1 inhibitor in patients with recurrent or progressive IDH1 mutant glioma: updated results from the phase 1 non-enhancing glioma population. Neuro Oncol 19(suppl 6):ACTR–A46. https://doi.org/10.1093/neuonc/nox168.037
14. Lowery MA, Abou-Alfa GK, Burris HA, Janku F, Shroff RT, Cleary JM, Azad NS, Goyal L, Maher EA, Gore L, Hollebecque A, Beeram M, Trent JC, Jiang L, Ishii Y, Auer J, Gliser C, Agresta SV, Pandya SS, Zhu AX (2017) Phase 1 study of AG-120, an IDH1 mutant enzyme inhibitor: results from the cholangiocarcinoma dose escalation and expansion cohorts. J Clin Oncol 35(suppl):A4015. https://doi.org/10.1200/JCO.2017.35.15_suppl.4015
15. US Food and Drug Administration (2018) FDA approves ivosidenib for relapsed or refractory acute myeloid leukemia. https://www.fda.gov/Drugs/InformationOnDrugs/ApprovedDrugs/ucm614128.htm. Accessed 1 Nov 2018
16. Dai D, DiNardo C, Stein E, de Botton S, Attar E, Liu H, Liu G, Lemieux I, Agresta S, Yang H, Fan B (2018) Clinical pharmacokinetics/pharmacodynamics (PK/PD) of ivosidenib in patients with IDH1-mutant advanced hematologic malignancies from a phase 1 study. J Clin Oncol 36(15):Abstr2581. https://doi.org/10.1200/JCO.2018.36.15_suppl.2581
17. Dai D, Yang H, Nabhan S, Hickman D, Liu G, Zacher J, Vutikullird A, Prakash C, Agresta S, Bowden C, Fan B (2019) Effect of itraconazole, food and ethnic origin on pharmacokinetics of ivosidenib in healthy subjects. Eur J Clin Pharmacol (**Under revision**)
18. Penner N, Xu L, Prakash C (2012) Radiolabeled absorption, distribution, metabolism, and excretion studies in drug development: why, when, and how? Chem Res Toxicol 25:513–531. https://doi.org/10.1021/tx300050f
19. Robison TW, Jacobs A (2009) Metabolites in safety testing. Bioanalysis 1:1193–1200. https://doi.org/10.4155/bio.09.98
20. The 2007 Recommendations of the International Commission on Radiological Protection (2007) ICRP publication. Ann ICRP 37:103. https://doi.org/10.1016/j.icrp.2007.10.003
21. Hamilton RA, Garnett WR, Kline BJ (1981) Determination of mean valproic acid serum level by assay of a single pooled sample. Clin Pharmacol Ther 29:408–413. https://doi.org/10.1038/clpt.1981.56
22. Prakash C, Shaffer CL, Nedderman A (2007) Analytical strategies for identifying drug metabolites. Mass Spectrom Rev 26:340–369. https://doi.org/10.1002/mas.20128
23. Zollinger M, Lozac'h F, Hurh E, Emotte C, Bauly H, Swart P (2014) Absorption, distribution, metabolism, and excretion (ADME) of (14)C-sonidegib (LDE225) in healthy volunteers. Cancer Chemother Pharmacol 74:63–75. https://doi.org/10.1007/s00280-014-2468-y